Operation Analysis and A Game Theoretic Approach to Dynamic Hybrid Compensator for the V/v Traction System

Zhen Zhu, Fujun Ma, Member, *IEEE*, Xin Wang, Lingfeng Deng, Gaoxiang Li, Xinwei Wei, Yuxuan Tang, Siyi Liu

***Abstract*—Due to the train load stochastic jumps, negative sequence currents are unpredictably brought into power grid, which may attack the power system and damage vital devices. To enhance the compensation capacities and improve the power quality, a hybrid scheme is studied in consideration of load stochastic jumps, composed of Railway Power Conditioner, Thyristor Switched Capacitor and Thyristor Switched Reactor. Firstly, the load discrete jump model and its compensation principle of V/v railway traction system are analyzed to design the hybrid compensators and the capacities. Then, based on the attack-defense game theory, a two-level optimized hybrid controller is proposed to keep the power system affirmative for any train load attacks. In the hybrid system, defender 1 is a discrete strategy that can be early executed by finite logic to minimize the power demands, and defender 2 is a continuous strategy that can be lately controlled by optimal control to minimize negative sequence currents. By this dynamic game, an optimized hybrid compensation can be realized. Finally, simulations and experiments are completed to prove the compensation abilities of the hybrid system and the effectiveness of the hybrid control strategy.**

***Index Terms*—Power Quality, Hybrid Compensation, Train Load Analysis, Game Theoretic Approach, Hybrid Control.**

I. INTRODUCTION

With the development of high-speed railway and traction power supply technology, the speed of trains reaches 300km/h or more, which brings great convenience to human society. As the high-speed electric locomotive is a high-power single-phase load, and the numbers of locomotives are varied on two traction arms, the three-phase grid currents are not easy to keep in balance with the varied loads. Those will bring some issues into power system, such as negative sequence currents (NSCs), reactive power and harmonics [1]-[10]. In decade years, there are lots of methods reducing the NSC to meet the standard in the electrified railway.

As to optimize the transformer, SCOTT transformer, IMBT, Leblanc transformer, power electronic transformer (PET) are used to decrease NSCs. At this moment, it is particularly worth mentioning that the PET integrated is a promising method to eliminate NSC with the advanced power electronics technology in the future [11]. In [12], the world's first power electronic traction transformer (PETT) has been newly developed, commissioned, and installed on the locomotive for the 15kV, 16 2/3Hz railway grid, which is presently in use by Europe countries. Meanwhile, [13] was concerned with the design of the input filter for a medium-frequency (MF) traction converter to minimize the filter's overall mass. By further reviewing all kinds of PET-based designs from the early concepts to the latest ones in the order of their publication dates, the developing trends are highlighted. And by considering the requirements and the state of the art synthetically, the key challenges and opportunities are identified and discussed [14].

As to add extra compensation elements, the equipments are mainly divided into two categories. One is single compensation elements and the other is hybrid compensation elements. As for single compensation system, passive filter (PF), active power filters (APF), static var compensator (SVC), static synchronous compensator (STATCOM) were commonly used [15]-[19]. Then, railway power conditioner (RPC) was proposed by scholars in 1993 [20], which consists of two back-to-back power converters, and two connected converters can control active and reactive currents to compensate NSCs synthetically. After that, a lot of improved topologies were proposed for the railway power system, such as active power quality compensator (APQC) [21], the structure of multiplexed RPC system and so on [22]-[24]. However, step-down transformers are required to connect multiple RPC systems with traction grid. In [25]-[27], new topologies of RPC were studied in compensating by using a two-phase modular multilevel converter (MMC) or a three-phase MMC, which can connect the power system directly. And in [28], for grid-connection compatibility and operating performance improvement, a capacity optimized

Manuscript received Jun 21, 2018; revised Oct 19, 2018; accepted Dec 05, 2018. This work was supported by the National Natural Science Foundation of China under Grant 51607062. (*Corresponding author: Fujun Ma.*)

Z. Zhu, F. Ma, X. Wang, L. Deng, G. Li, X. Wei, Y. Tang, S. Liu are with the College of Electrical and Information Engineering, Hunan University, Changsha 410082, China (e-mail: 332120507@qq.com; mafujun2004@163.com; 625661800@qq.com; 2982766254@qq.com; 1511872579@qq.com; 1205803198@qq.com; yx41tyx@sina.com; 1172065004@qq.com).

Color versions of one or more of the figures in this paper are available online at http://ieeexplore.ieee.org.

Digital Object Identifier 10.1109/TPEL.2018.xxxxxxx

strategy is focused in terms of both the utility and the train supply networks. In [29], to operate in a maximum compensating mode (MCM), a flexible fractional compensating mode (FrCM) was presented and its corresponding control system to mitigate the required rating of RPC. Nevertheless, the high compensation capacity and the investment cost of RPCs are limited to its further promotion. For a lower cost or a larger capacity, some hybrid compensation systems were proposed. In [30] and [31], a hybrid compensation is accomplished, based on SVC+RPC. In [32]-[34], the topologies of the "hybrid" RPCs are presented, which can reduce the capacity of active part. In [35], an asymmetrical connection balance transformer-based hybrid railway power conditioning system (ACBT-HRPC) was proposed with considering the cost function optimization for a lower cost. In [36], a system with series hybrid converter and shunt active converter (SHC&SAC) was proposed for compensation in co-phase high-speed electric railways. In [37]-[38], a hybrid traction power quality compensation system (HTPQCS) and a novel topology of hybrid railway power conditioner (H-RPC) were proposed, respectively. In [39], a combined system of a thyristor-controlled reactor (TCR) and a shunt hybrid power filter (SHPF) were proposed for harmonic and reactive power compensation. All the above hybrid topologies have improved the compensation abilities. However, there are still few researches considering the probable train loads of two traction arms, which is the essential for the unbalance of the three-phase grid currents. So this paper is motivated to improve the dynamic performance of hybrid compensation system in consideration of the train load random jumps.

Hybrid controllers can be designed by automata, peri nets, the optimal control methods, hierarchical control methods, distributed, multi-agent control methods and so on [40]-[44]. All these methods have already been applied in the engineering. While the game theory can't wait to extend the special values, as it provides a powerful means for modeling the cooperation and interaction of different decision players [45]-[46]. In [47], a general system structure consists of a set of local controllers and a game-theoretic supervisory control constructed in the framework of discrete-event systems (DES). In [48], a game-theoretic scheme based on the Nash equilibrium (NE) is used to coordinate appliance operations in a residential building. And in [49], a game-theoretic MPC was proposed for demand side energy management. In this paper, based on the attack-defense game theory, a two-level optimized hybrid controller is successfully designed to realize the coordinated compensation for RPCs, Thyristor Switched Capacitor (TSCs) and Thyristor Switched Reactor (TSRs).

The structure of this paper is as follows. In section II, the discrete locomotive mathematical model of railway system is analyzed, and the compensation demands of the active and reactive power are figured out. On the basis of the discrete locomotive model, the design of dynamic hybrid compensator is studied in section III. In section IV, based on the attack-defense game, a hybrid controller of the discrete switches of TSCs, TSRs and the continuous currents of RPCs are implemented. Finally, verifications and conclusions will be conducted in Section V and VI, respectively.

II. The Load Discrete Model and Power Demand Analysis

As the high-speed V/v traction system in China, the primary and secondary side of transformer is 220kV and 2 × 27.5kV, shown in Fig. 1. If the autotransformers (ATs) are considered, contact wire (+27.5kV) and feeder wire (-27.5kV) are connected with the auto-transformer (AT) directly, which make up the 55kV power supply system, and the train rail is connected with the neutral line of AT, which remains 27.5 kV between contact wire and the train rail. As the speed of the locomotive is 300 km/h or more, and the minimum tracking interval is 3 minutes, for safety, two locomotives are at most allowed to go straight the same line together. What's more, as the high-speed railway system adapts double lines, there are 5×5=25 combinations of the probable train loads in the traction power system.

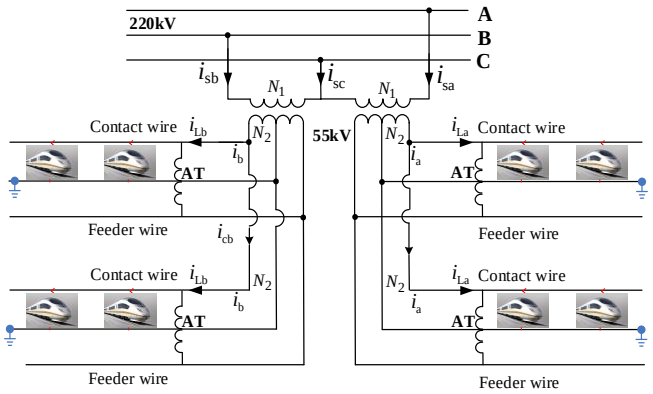

Fig. 1. Double-line traction mode for V/v traction power supply system.

The high-speed railway locomotives are often driven by four-quadrant PWM converters, and power factor of two feeder sections is nearly 1. Caused by the inherited single-phase traction mode, three-phase unbalanced current is serious and changed dynamically due to the varying train loads, which must be governed. To eliminate the unbalanced currents of V/v system [50], the transferring of active power and the compensation of reactive power can be calculated as

$$\begin{cases} P_a' = -P_b' = \dfrac{P_a - P_b}{2} \\ Q_a' = \dfrac{P_a + P_b}{2}\tan 30^\circ \\ Q_b' = -\dfrac{P_a + P_b}{2}\tan 30^\circ \end{cases} \tag{1}$$

Where P_a, P_b are the train load power of a-phase traction arm and b-phase traction arm; P_a', P_b' are the active power needed to be transferred; Q_a', Q_b' are the reactive power needed to be compensated. Based on the probable load combinations of the double-line traction system, the compensation demands of the active power and reactive power for phase-a and b traction arms can be calculated in Table I.

In Table I, (N_a, N_b) means the train number of two traction

arms; M is the capacity of single train load, while *S* is the apparent power. If the demands of the active and reactive power of a-phase and b-phase arms for compensation are represented as ($P_a^{'}$, $Q_a^{'}$) and ($P_b^{'}$, $Q_b^{'}$), then a power coordinate frame can be obtained as shown in Fig. 2.

Table I The compensation demands of the active and reactive power under different train loads

(N_a, N_b)	a-arm		b-arm		
	P_a'	Q_a'	P_b'	Q_b'	*S*
(0,0)	0	0	0	0	0
(0,1)	-M/2	$\sqrt{3}$M/6	M/2	$-\sqrt{3}$M/6	0.577M
(0,2)	-M	$\sqrt{3}$M/3	M	$-\sqrt{3}$M/3	1.155M
(0,3)	-3M/2	$\sqrt{3}$M/2	3M/2	$-\sqrt{3}$M/2	1.732M
(0,4)	-2M	$2\sqrt{3}$M/3	2M	$-2\sqrt{3}$M/3	2.309M
(1,0)	M/2	$\sqrt{3}$M/6	-M/2	$-\sqrt{3}$M/6	0.577M
(1,1)	0	$\sqrt{3}$M/3	0	$-\sqrt{3}$M/3	0.577M
(1,2)	-M/2	$\sqrt{3}$M/2	M/2	$-\sqrt{3}$M/2	1M
(1,3)	-M	$2\sqrt{3}$M/3	M	$-2\sqrt{3}$M/3	1.528M
(1,4)	-3M/2	$5\sqrt{3}$M/6	3M/2	$-5\sqrt{3}$M/6	2.082M
(2,0)	M	$\sqrt{3}$M/3	-M	$-\sqrt{3}$M/3	1.155M
(2,1)	M/2	$\sqrt{3}$M/2	-M/2	$-\sqrt{3}$M/2	1M
(2,2)	0	$2\sqrt{3}$M/3	0	$-2\sqrt{3}$M/3	1.155M
(2,3)	-M/2	$5\sqrt{3}$M/6	M/2	$-5\sqrt{3}$M/6	1.528M
(2,4)	-M	$\sqrt{3}$M	M	$-\sqrt{3}$M	2M
(3,0)	3M/2	$\sqrt{3}$M/2	-3M/2	$-\sqrt{3}$M/2	1.732M
(3,1)	M	$2\sqrt{3}$M/3	-M	$-2\sqrt{3}$M/3	1.528M
(3,2)	M/2	$5\sqrt{3}$M/6	-M/2	$-5\sqrt{3}$M/6	1.528M
(3,3)	0	$\sqrt{3}$M	0	$-\sqrt{3}$M	1.732M
(3,4)	-M/2	$7\sqrt{3}$M/6	M/2	$-7\sqrt{3}$M/6	2.082M
(4,0)	2M	$2\sqrt{3}$M/3	-2M	$-2\sqrt{3}$M/3	2.309M
(4,1)	3M/2	$5\sqrt{3}$M/6	-3M/2	$-5\sqrt{3}$M/6	2.082M
(4,2)	M	$\sqrt{3}$M	-M	$-\sqrt{3}$M	2M
(4,3)	M/2	$7\sqrt{3}$M/6	-M/2	$-7\sqrt{3}$M/6	2.082M
(4,4)	0	$4\sqrt{3}$M/3	0	$-4\sqrt{3}$M/3	2.309M

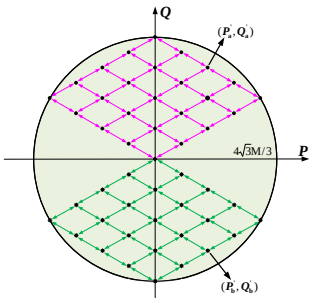

Fig. 2. The power coordinate with considering the probable train loads.

In Fig. 2, each dot represents one status of the 25 probable train load combinations. Each jump indicates that the system has been changed and it can be described as the load discrete model. If these dots are surrounded by a circle, the power demands of compensation system can be obtained and it reaches to $4\sqrt{3}$M/3 , which is in want of a large capacity of power compensation. What's more, it can be found that the statuses of a-phase arm are all above the horizontal axis (Q>0) and the statuses of b-phase arm are all below the horizontal axis (Q<0), which means phase-a traction power arm needs the capacitive reactive power and phase-b traction power arm needs the inductance reactive power. Thus, if we use the capacitive elements (such as TSC) installed on a-phase arm and the inductance elements (such as TSR) installed on b-phase arm, the power quality will be improved. To this point, a hybrid system is designed to enhance the compensation resilience with all probable train load jumps.

III. The Design of Hybrid Compensation System

If the traction system is compensated by RPCs, the demand of the compensation capacity is large and once one component of RPCs falls toward a fault unfortunately, the compensation system will not be enabled to keep the grid currents balanced for all operation statuses, shown in Fig. 3(a). The power capacity of RPC system is reduced from the dashed circle to the solid circle, some load operation statuses cannot be fully compensated.

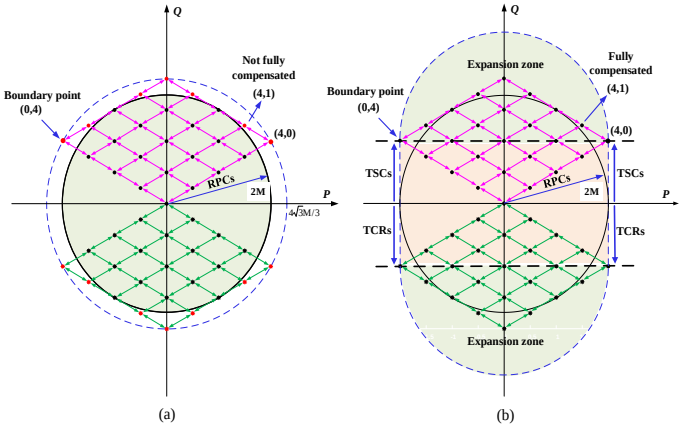

Fig. 3. Power coordinates with different compensation system. (a) RPCs. (b) RPCs+TSCs+TSRs.

But if TSCs and TSRs, the cost of which is lower, are also considered in the compensation system, some conditions will be changed, shown in Fig. 3(b). TSCs and TSRs can expand the small solid circle of RPCs to two semi-circles and the compensation zone is enlarged. As a result, all the dots are surrounded. So, the hybrid compensation system can enhance power system resilience, which is composed of RPCs, TSCs and TSRs.

In Fig. 3(b), it can be found that the maximum active power is 2M and the maximum reactive power is $4\sqrt{3}$M/3 . As the active power can only be transferred by RPCs, so 10 sets of RPCs can be designed and the capacity of each RPC is 0.2M. In the meantime, the reactive power can be compensated by RPCs, TSCs and TSRs, but RPCs are mainly purposed to transfer the active power, so the total capacities of TSCs and TSRs could be $4\sqrt{3}$M/3 . To reduce the number of TSCs and TSRs, different capacities of each component can be considered. Based on Table I, 4 sets of TSCs and TSRs can be designed, that is, 2 sets with the capacity of $\sqrt{3}$M/6 , 1 set with the capacity of $\sqrt{3}$M/3 , 1 set with the capacity of $2\sqrt{3}$M/3 . As the capacitive elements

installed on a-phase arm and the inductance elements installed on b-phase arm are symmetrical, the capacities of TSCs and TSRs are the same. At this point, the hybrid system can be designed as shown in Fig. 4.

The parameters are listed in Table II, where, N_a and N_b are the number of the trains, discrete variables; i_{ca} and i_{cb} are the currents of RPCs, continuous variables; $S_{TSC1,2,3,4}$ and $S_{TSR1,2,3,4}$ represent the switches of TSCs and TSRs, discrete variables.

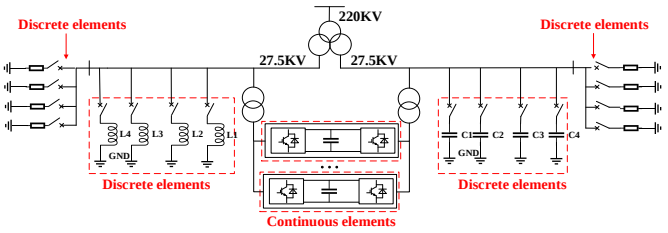

Fig. 4. Schematic of hybrid compensation systems.

Table II The parameters of hybrid compensation systems

Elements	Power(MW)	Number	Main parameters	Event
Train	M	(4,4)	N_a, N_b	Discrete
RPCs	0.2M	10	i_{ca},i_{cb}	Continuous
TSC1	$\sqrt{3}$M/6	1	S_{TSC1}	Discrete
TSC2	$\sqrt{3}$M/6	1	S_{TSC2}	Discrete
TSC3	$\sqrt{3}$M/3	1	S_{TSC3}	Discrete
TSC4	$2\sqrt{3}$M/3	1	S_{TSC4}	Discrete
TSR1	$\sqrt{3}$M/6	1	S_{TSR1}	Discrete
TSR2	$\sqrt{3}$M/6	1	S_{TSR2}	Discrete
TSR3	$\sqrt{3}$M/3	1	S_{TSR3}	Discrete
TSR4	$2\sqrt{3}$M/3	1	S_{TSR4}	Discrete

In Fig. 4, the equivalent circuits of the hybrid system can be obtained and shown in Fig. 5.

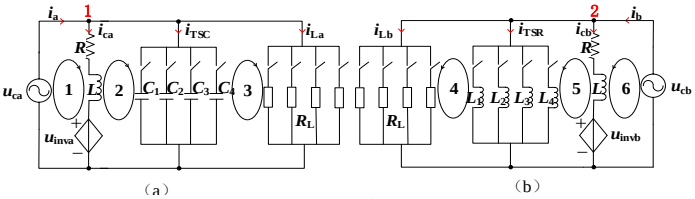

Fig. 5. Equivalent circuit of the hybrid system.

Based on the loops in Fig. 5, the system can be mathematically modeled and validated by KVL, and there is

$$\begin{cases} i_{La} = N_a \dfrac{u_{ca}}{R_L} \\ i_{Lb} = N_b \dfrac{u_{cb}}{R_L} \end{cases} \tag{2}$$

$$\begin{cases} i_{TSC1} = S_{TSC1} C_1 \dfrac{du_{ca}}{dt} \\ \vdots \\ i_{TSC4} = S_{TSC4} C_4 \dfrac{du_{ca}}{dt} \end{cases} \tag{3}$$

$$\begin{cases} u_{cb} = S_{TSR1} L_1 \dfrac{di_{TSR1}}{dt} \\ \vdots \\ u_{cb} = S_{TSR4} L_4 \dfrac{di_{TSR4}}{dt} \end{cases} \tag{4}$$

$$\begin{cases} u_{ca} = L \dfrac{di_{ca}}{dt} + i_{ca} R + u_{inva} \\ u_{cb} = L \dfrac{di_{cb}}{dt} + i_{cb} R + u_{invb} \end{cases} \tag{5}$$

Where, u_{ca}, u_{cb} are the voltages of two arms in traction power system; R_L, i_{La} and i_{Lb} are represented as the equivalent resistance and currents of the train loads in two traction arms; $C_{1,2,3,4}$ and $i_{TSC1,2,3,4}$ are the capacitances and the currents of TSCs; $L_{1,2,3,4}$ and $i_{TSR1,2,3,4}$ are the inductances and the currents of TSRs; u_{inva}, u_{invb}, i_{ca} and i_{cb} are the equivalent output voltages and currents of RPCs in two traction arms.

Based on KCL for Nodes 1 and 2, the equation can be derived as

$$\begin{cases} i_a = i_{La} + i_{TSC} + i_{ca} \\ i_b = i_{Lb} + i_{TSR} + i_{cb} \end{cases}. \tag{6}$$

Then, the three-phase grid currents can be obtained with the following equation, that is

$$\begin{bmatrix} i_{sa} \\ i_{sb} \\ i_{sc} \end{bmatrix} = \frac{1}{K} \begin{bmatrix} 1 & 0 \\ 0 & 1 \\ -1 & -1 \end{bmatrix} \begin{bmatrix} i_a \\ i_b \end{bmatrix}. \tag{7}$$

By (2)-(7), it can be found that the currents of each element are coupling. That is, those components of the hybrid system are not independent and they interact with each other to impact the three-phase grid currents synchronously. For example, the train loads are dynamic stochastic jumps, TSCs, TSRs are frequently switched or RPCs' currents are continuously changed and so on. All the actions will greatly affect the power quality of the railway grid. Once one component or more are lonely controlled or executed without valid cooperation, unfortunately, they will meet failure together. So, a safe and reliable controller will be designed and it cannot be halted.

IV. Game Theoretic Approach For Hybrid Control

The traction power system can be seen as a game between two players: one is the attackers, that is, the probable train loads, which break the current balance; the other is the defenders, including RPCs, TSCs and TSRs, which are designed to keep the current balanced for any unfriendly attacks. The dynamic game tree between the probable train loads and the hybrid compensator can be shown in Fig. 6.

The attackers and the defenders are a dynamic zero-sum game, that is, the loss of one side is the gain of the other. If the value function of one party is determined, the value functions of both parties are determined.

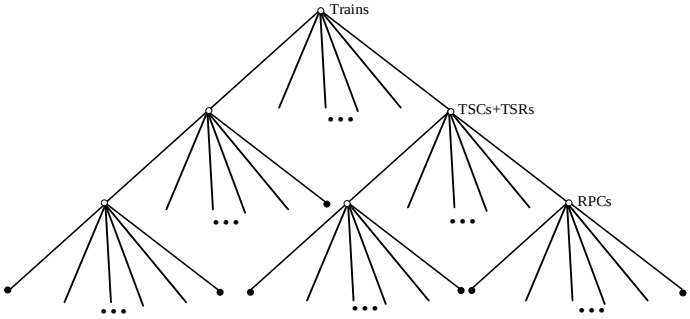

Fig. 6. The dynamic game tree of trains, TSCs, TSRs and RPCs.

The utility functions J of the hybrid compensation system can be calculated as follows:

$$\min J = \frac{|I_-|}{|I_+|} = \frac{\left|\frac{1}{3}(\dot{I}_A + \alpha^2 \dot{I}_B + \alpha \dot{I}_C)\right|}{\left|\frac{1}{3}(\dot{I}_A + \alpha \dot{I}_B + \alpha^2 \dot{I}_C)\right|} \times 100\% \quad (8)$$

Where, I_-, I_+ are represented as the negative and positive sequence currents, respectively, and $\alpha = e^{j120^0}$. I_-, I_+ can be calculated as follows:

$$I_- = \frac{1}{3}\left(\frac{\sqrt{3}}{2} I_{La} - \sqrt{3} I_{Lb} + \frac{3\sqrt{3}}{2} I_{RPCp} + \frac{3}{2} I_{RPCqa} + \frac{3}{2} I_{TSC}\right) + \frac{1}{3}\left(-\frac{3}{2} I_{La} - \frac{3}{2} I_{RPCp} + \frac{\sqrt{3}}{2} I_{RPCqa} + \sqrt{3} I_{RPCqb} + \frac{\sqrt{3}}{2} I_{TSC} + \sqrt{3} I_{TSR}\right) \times i \quad (9)$$

$$I_+ = \frac{1}{3}\left(\sqrt{3}\left(I_{La} + I_{Lb}\right) + \sqrt{3}\left(I_{RPCqa} - I_{RPCqb} + I_{TSC} - I_{TSR}\right) \times i\right) \quad (10)$$

Where, I_{La} and I_{Lb} are represented as the root mean square (RMS) of two train-load currents; I_{RPCp}, I_{RPCqa} and I_{RPCqb} are represented as the RMS of transferred active currents and compensated reactive currents of RPCs; I_{TSC} and I_{TSR} are represented as the RMS of output currents of TSCs and TSRs respectively.

If there is no train entering or going by, the hybrid compensation system has already been operated in the steady-state and the three-phase grid currents are kept in balance. Once a locomotive (the attacker) enters or goes by, the hybrid compensation system should also be appropriately changed to keep the three-phase currents balanced. The hybrid control can be divided into two layers. In the first layer, TSCs and TSRs (defender 1) are compensated to minimize the power demands J_1 of RPCs. And in the second layer, RPCs (defender 2) will be executed to minimize the negative sequence current J_2.

A. Attacker: Stochastic jumps of the train load

The ac train is supplied by AC four-quadrant PWM rectifier generally, and the power factor is close to 1. Meanwhile, the low harmonic content is greatly reduced. Due to the high-power of high-speed electric locomotives and the single-phase traction mode, the negative-sequence currents generated is more serious than that of ordinary electrified railway. On the analysis of section II and for the safety requirement, 4 trains are the maximum in each power supply traction arm simultaneously. Different train loads on two traction lines may lead to different attacks. So, 25 strategies can be taken by the attacker to break the balance of three-phase grid currents. What's more, the attack strategies of the attacker are stochastic in the game.

B. Defender 1: TSCs and TSRs

As the train load jump is certain at some time randomly, the decisions of TSCs and TSRs should also be done correspondingly to defense the traction power system. But based on the imaginary part of (9), for a good power factor, the positive-sequence reactive currents should be zero and I_{TSC}, I_{TSR}, I_{RPCqa}, I_{RPCqb} should be correlated. If the reactive compensation of TSCs and TSRs are not the same, RPCs will need to compensate a certain quantity of reactive power to neutralize the positive-sequence reactive currents, which is not good for the optimal operation of RPCs in the next step. So, the reactive compensation of TSCs and TSRs should be the same. There is

$$I_{TSC} = I_{TSR} \quad (11)$$

By (11), some elements of TSCs and TSRs could work together, that is, TSC1 and TSR1, TSC2 and TSR2, TSC3 and TSR3, TSC4 and TSR4, which can be labeled as the sub-module I, II, III and IV. Thus, the combinations are cut down to reduce the complexity. Considering the total capacities, 9 cases for TSCs and TSRs can be analyzed as shown in Table III.

Table III The combinations of TSCs or TSRs

Total capacities/ p.u.	0	1	2	3	4	5	6	7	8
The combinations	-	I	II	I, III	IV	I, IV	II, IV	I,III, IV	I,II,III, IV

To realize the maximum defense and the minimum attack, in the first layer, the minimum power demands for RPCs can be regarded as the cost function after defender 1's decision.

$$J_1 = \min \sqrt{I_{RPCp}^2 + I_{RPCqa,b}^2} \quad (12)$$

After the first defense of TSCs and TSRs, the power demands J_1 for RPCs can be listed in Table IV.

In Table IV, there are 25 strategies for attacker and 9 strategies for defender 1. When attacker takes an action, that is, a train enters or leaves, the original balanced system will be broken and some unbalanced currents will be brought into. To minimize the unbalanced currents, defender 1 can take a wise action by Table III and Table IV. For example, if the attacker makes an attack that one train is in phase-a arm and two trains are in phase-b arm, that is (1,2), to minimize the unbalanced currents, defender 1 should compensate 3 p.u. reactive powers. Namely, TSC1, TSR1 and TSC3, TSR3 should be switched on the working mode based on Table III. One attack reflects one defense. So, the actions of defender 1 can be obtained by Table III and Table IV to achieve the maximum defense for attacks. It can be described as (S_{TSC}^*, S_{TSR}^*).

In addition, in the process of switching on-off, TSCs and TSRs should not create the voltage or current transients. According to (3), TSCs should be switched on-off at the negative and positive peak value of traction voltage to avoid current transients. It can be accomplished by measuring the voltage of the thyristor. When the voltage of the thyristor is zero, it can be switched on or off. At the same time, according to (4), TSRs should be switched on or off when the current is across 0 point.

C. Defender 2: RPCs

After the defender 1's defense, the level of three-phase unbalance will be reduced. But if only defender 1 defenses the attacker, it cannot be a complete defense, because TSCs and TSRs can just compensate the reactive power, not able to transfer the active power. Furthermore, TSCs and TSRs can only discretely compensate the reactive power, which isn't precise for every stochastic train load jump. As a result, RPCs of defender 2 is inevitable to transfer the active power and compensate the remaining reactive power. Firstly, the expected references of the active and reactive currents are obtained, and then the optimal control is studied to implement the current tracking.

As the capacity of RPCs are restricted, it can be described as follows:

Table IV The stochastic train load versus TSCs, TSRs game

		Defender 1 (TSRs+TSCs)								
		0 p.u.	1 p.u.	2 p.u.	3 p.u.	4 p.u.	5 p.u.	6 p.u.	7 p.u.	8 p.u.
Attacker (Trains)	(0,0)	**0.000** M	0.288 M	0.577M	0.866M	1.155M	1.443M	1.732M	2.020M	2.309M
	(0,1)	0.577 M	**0.500** M	0.577M	0.763M	1.000M	1.259M	1.527M	1.803M	2.081M
	(0,2)	1.155 M	1.040 M	**1.000** M	1.040 M	1.155 M	1.323 M	1.528 M	1.756 M	2.000 M
	(0,3)	1.732 M	1.607 M	1.527 M	**1.500** M	1.527 M	1.607 M	1.732 M	1.893 M	2.081 M
	(0,4)	2.309 M	2.179 M	2.081 M	2.020 M	**2.000** M	2.020 M	2.081 M	2.179 M	2.309 M
	(1,0)	0.577 M	**0.500** M	0.577 M	0.763 M	1.000 M	1.259 M	1.527 M	1.803 M	2.081 M
	(1,1)	0.577 M	0.288 M	**0.000** M	0.288 M	0.577 M	0.866 M	1.155 M	1.443 M	1.732 M
	(1,2)	1.000 M	0.763 M	0.577 M	**0.500** M	0.577 M	0.763 M	1.000 M	1.259 M	1.527 M
	(1,3)	1.528 M	1.323 M	1.155 M	1.040 M	**1.000** M	1.040 M	1.155 M	1.323 M	1.528 M
	(1,4)	2.082 M	1.893 M	1.732 M	1.607 M	1.527 M	**1.500** M	1.527 M	1.607 M	1.732 M
	(2,0)	1.155 M	1.040 M	**1.000** M	1.040 M	1.155 M	1.323 M	1.528 M	1.756 M	2.000 M
	(2,1)	1.000 M	0.763 M	0.577 M	**0.500** M	0.577 M	0.763 M	1.000 M	1.259 M	1.527 M
	(2,2)	1.155 M	0.866 M	0.577 M	0.288 M	**0.000** M	0.288 M	0.577 M	0.866 M	1.155 M
	(2,3)	1.528 M	1.259 M	1.000 M	0.763 M	0.577 M	**0.500** M	0.577 M	0.763 M	1.000 M
	(2,4)	2.000 M	1.756 M	1.528 M	1.323 M	1.155 M	1.040 M	**1.000** M	1.040 M	1.155 M
	(3,0)	1.732 M	1.607 M	1.527 M	**1.500** M	1.527 M	1.607 M	1.732 M	1.893 M	2.082 M
	(3,1)	1.528 M	1.323 M	1.155 M	1.040 M	**1.000** M	1.040 M	1.155 M	1.323 M	1.528 M
	(3,2)	1.528 M	1.259 M	1.000 M	0.763 M	0.577 M	**0.500** M	0.577 M	0.763 M	1.000 M
	(3,3)	1.732 M	1.443 M	1.155 M	0.866 M	0.577 M	0.288 M	**0.000** M	0.288 M	0.577 M
	(3,4)	2.082 M	1.803 M	1.528 M	1.259 M	1.000 M	0.763 M	0.577 M	**0.500** M	0.577 M
	(4,0)	2.309 M	2.179 M	2.081 M	2.020 M	**2.000** M	2.020 M	2.081 M	2.179 M	2.309 M
	(4,1)	2.082 M	1.893 M	1.732 M	1.607 M	1.527 M	**1.500** M	1.527 M	1.607 M	1.732 M
	(4,2)	2.000 M	1.756 M	1.528 M	1.323 M	1.155 M	1.040 M	**1.000** M	1.040 M	1.155 M
	(4,3)	2.082 M	1.803 M	1.528 M	1.259 M	1.000 M	0.763 M	0.577 M	**0.500** M	0.577 M
	(4,4)	2.309 M	2.020 M	1.732 M	1.443 M	1.155 M	0.866 M	0.577 M	0.288 M	**0.000** M

$$\begin{cases} I_{\mathrm{RPCp}}^2 + I_{\mathrm{RPCqa}}^2 \le \varsigma^2 I_{\mathrm{RPC}}^2 \\ I_{\mathrm{RPCp}}^2 + I_{\mathrm{RPCqb}}^2 \le \varsigma^2 I_{\mathrm{RPC}}^2 \end{cases} \tag{13}$$

Where I_{RPCp}, I_{RPCqa}, I_{RPCqb} are the active current, reactive currents of a-phase and b-phase traction arm, respectively; ς is the residual rate of RPCs' capacity after some elements' failure. As the active power of positive sequence current I_+ is determined by the train loads, and the reactive power is basically zero after defender 1's actions, the negative sequence current I_- can be taken as the cost function in the second level.

$$J_2 = \min |I_-| \tag{14}$$

To minimize negative sequence currents, Lagrange function can be obtained with the constraint condition (10), and there is

$$L = \left|I^-\right|^2 + \lambda_1\left(I_{\mathrm{RPCp}}^2 + I_{\mathrm{RPCqa}}^2 - I_{\mathrm{RPC}}^2\right) + \lambda_2\left(I_{\mathrm{RPCp}}^2 + I_{\mathrm{RPCqb}}^2 - I_{\mathrm{RPC}}^2\right) \tag{15}$$

By the law of K-T conditions, the necessary conditions can be obtained by the existence of the optimal solutions, there is,

$$\begin{cases} \dfrac{\partial L}{\partial I_{\mathrm{RPCp}}} = I_{\mathrm{La}} - I_{\mathrm{Lb}} + \dfrac{\sqrt{3}}{3}\left(I_{\mathrm{RPCqa}} - I_{\mathrm{RPCqb}}\right) + 2\left(\lambda_1 + \lambda_2 + 1\right) I_{\mathrm{RPCp}} = 0 \\ \dfrac{\partial L}{\partial I_{\mathrm{RPCqa}}} = -\dfrac{\sqrt{3}}{3} I_{\mathrm{Lb}} + \dfrac{\sqrt{3}}{3} I_{\mathrm{RPCp}} + \dfrac{2}{3} I_{\mathrm{RPCqa}} + \dfrac{1}{3} I_{\mathrm{RPCqb}} + 2\lambda_1 I_{\mathrm{RPCqa}} = 0 \\ \dfrac{\partial L}{\partial I_{\mathrm{RPCqb}}} = -\dfrac{\sqrt{3}}{3} I_{\mathrm{La}} - \dfrac{\sqrt{3}}{3} I_{\mathrm{RPCp}} + \dfrac{1}{3} I_{\mathrm{RPCqa}} + \dfrac{2}{3} I_{\mathrm{RPCqb}} + 2\lambda_2 I_{\mathrm{RPCqb}} = 0 \\ \lambda_1\left(\varsigma^2 I_{\mathrm{RPCp}}^2 + I_{\mathrm{RPCqa}}^2 - I_{\mathrm{RPC}}^2\right) = 0 \\ \lambda_2\left(\varsigma^2 I_{\mathrm{RPCp}}^2 + I_{\mathrm{RPCqb}}^2 - I_{\mathrm{RPC}}^2\right) = 0 \\ \lambda_1 \ge 0; \lambda_2 \ge 0 \end{cases} \tag{16}$$

Where, λ_1, λ_2 are Lagrange multipliers. If the capacity of RPCs is big enough and without fault, that is, ς=1, the traction power system can be fully compensated and K-T points can be deduced as follows:

This article has been accepted for publication in a future issue of this journal, but has not been fully edited. Content may change prior to final publication. Citation information: DOI 10.1109/TPEL.2018.2887226, IEEE Transactions on Power Electronics

$$\begin{cases} I_{\mathrm{RPCp}}{}^{*} = \dfrac{I_{\mathrm{Lb}} - I_{\mathrm{La}}}{2} \\ I_{\mathrm{RPCqa}}{}^{*} = \dfrac{I_{\mathrm{La}} + I_{\mathrm{Lb}}}{2\sqrt{3}} - I_{\mathrm{TSC}} \\ I_{\mathrm{RPCqb}}{}^{*} = \dfrac{I_{\mathrm{La}} + I_{\mathrm{Lb}}}{2\sqrt{3}} - I_{\mathrm{TSR}} \end{cases} \tag{17}$$

The vector diagram can be drawn in Fig. 7. In Fig. 7(a), the train-load currents I_{La} and I_{Lb} make the three-phase grid currents unbalanced, but after the compensation currents I_{TSC} and I_{TSR} and the compensation currents I_{RPC} composed of I_{RPCp}, I_{RPCqa} and I_{RPCqb}, three-phase grid currents I_{A}, I_{B}, I_{C} are re-balanced.

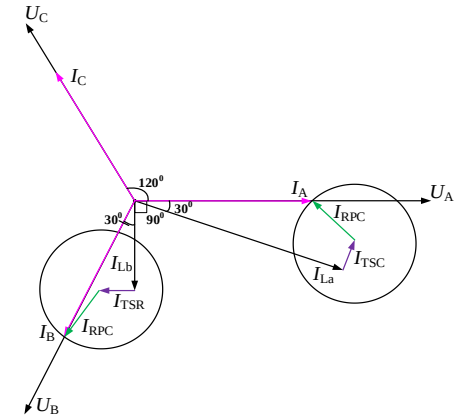

(a)

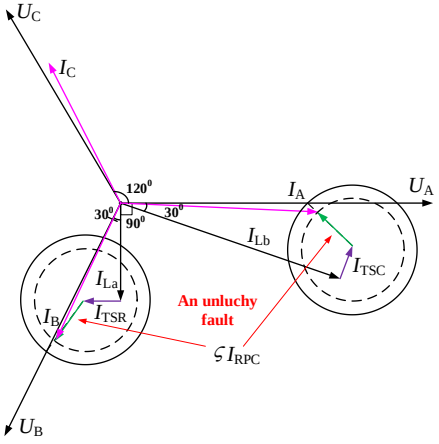

(b)

Fig. 7. Compensation of RPCs for traction power supply system. (a) Full compensation of RPCs. (b) Optimal compensation of RPCs.

Based on (17), $\varsigma I_{\mathrm{RPC}}$ should be satisfied with the inequations

$$\begin{aligned} \varsigma I_{\mathrm{RPC}} &\geq \sqrt{(I^{*}_{\mathrm{RPCpa}})^2 + (I^{*}_{\mathrm{RPCqa}})^2} \\ &= \sqrt{\frac{I_{\mathrm{La}}^2 + I_{\mathrm{Lb}}^2 - I_{\mathrm{La}} I_{\mathrm{Lb}} - \sqrt{3} I_{\mathrm{TSC}} (I_{\mathrm{La}} + I_{\mathrm{Lb}})}{3}} \end{aligned} \tag{18}$$

If the capacity of RPCs is limited or some sets of RPCs fall toward a fault ($\varsigma < 1$), in which the system cannot fully compensate the system and the inequations are not satisfied, the traction power system can be compensated optimally. By solving (16), the similar optimal compensation K-T points can be obtained, and there is

$$\begin{cases} I_{\mathrm{RPCp}}{}^{*} = \dfrac{\varsigma I_{\mathrm{RPC}}}{\sqrt{\dfrac{I_{\mathrm{La}}^2 + I_{\mathrm{Lb}}^2 - I_{\mathrm{La}} I_{\mathrm{Lb}} - \sqrt{3} I_{\mathrm{TSC}} (I_{\mathrm{La}} + I_{\mathrm{Lb}})}{3}}} \times \dfrac{(I_{\mathrm{Lb}} - I_{\mathrm{La}})}{2} \\ I_{\mathrm{RPCqa}}{}^{*} = \dfrac{\varsigma I_{\mathrm{RPC}}}{\sqrt{\dfrac{I_{\mathrm{La}}^2 + I_{\mathrm{Lb}}^2 - I_{\mathrm{La}} I_{\mathrm{Lb}} - \sqrt{3} I_{\mathrm{TSC}} (I_{\mathrm{La}} + I_{\mathrm{Lb}})}{3}}} \times \left(\dfrac{I_{\mathrm{La}} + I_{\mathrm{Lb}}}{2\sqrt{3}} - I_{\mathrm{TSC}} \right) \\ I_{\mathrm{RPCqb}}{}^{*} = \dfrac{\varsigma I_{\mathrm{RPC}}}{\sqrt{\dfrac{I_{\mathrm{La}}^2 + I_{\mathrm{Lb}}^2 - I_{\mathrm{La}} I_{\mathrm{Lb}} - \sqrt{3} I_{\mathrm{TSC}} (I_{\mathrm{La}} + I_{\mathrm{Lb}})}{3}}} \times \left(\dfrac{I_{\mathrm{La}} + I_{\mathrm{Lb}}}{2\sqrt{3}} - I_{\mathrm{TSR}} \right). \end{cases} \tag{19}$$

Based on (19), the unbalanced level of three-phase currents is minimized. The vector diagram can be drawn in Fig.6(b). In Fig. 6(b), the train-load currents I_{La} and I_{Lb} and the compensation currents I_{TSC} and I_{TSR} are the same in Fig. 6(a). While the residual rate of RPCs capacity ς is unlucky decreased, and the system can be compromised to optimal compensate. Combining (17) with (19), optimal actions of defender 2 can be obtained by minimizing the negative sequence current (J_2), that is ($I^{*}_{\mathrm{RPCp}}, I^{*}_{\mathrm{RPCqa}}, I^{*}_{\mathrm{RPCqb}}$).

What's more, to improve the performance of the control method, the linear quadratic regulator (LQR) control in the dq frame is accomplished in the following part. Based on the 1st and 6th loops in Fig. 5, the equivalent circuits of RPCs can be obtained shown in Fig. 8.

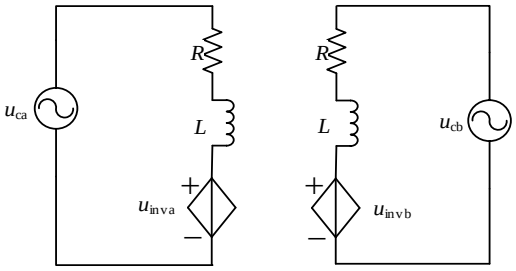

（a） （b）

Fig. 8. The equivalent circuits of RPCs. (a) a-phase arm. (b) b-phase arm.

The equivalent circuit of RPCs on the a-phase traction arm can be shown in Fig. 8(a), and based on the KCL law, the equation can be obtained in the **α**-β frame. There is

$$u_{\mathrm{ca}} = L\frac{di_{\mathrm{ca}}}{dt} + i_{\mathrm{ca}}R + u_{\mathrm{inva}} \tag{20}$$

Where u_{inva} is the equivalent voltage of the phase-a inverter. Transforming (20) into a single-phase dq frame, and there is

$$\begin{cases} L\dfrac{di_{\mathrm{cad}}}{dt} = -i_{\mathrm{cad}}R + \omega L i_{\mathrm{caq}} + u_{\mathrm{cad}} - u_{\mathrm{invad}} \\ L\dfrac{di_{\mathrm{caq}}}{dt} = -i_{\mathrm{caq}}R - \omega L i_{\mathrm{cad}} - u_{\mathrm{invaq}} \end{cases} \tag{21}$$

In the same way, the equivalent circuit of RPCs on b-phase traction arm can be shown in Fig. 8(b). There is

This article has been accepted for publication in a future issue of this journal, but has not been fully edited. Content may change prior to final publication. Citation information: DOI 10.1109/TPEL.2018.2887226, IEEE Transactions on Power Electronics

$$\begin{cases} L\dfrac{di_{\mathrm{cbd}}}{dt} = -i_{\mathrm{cbd}}R + \omega L i_{\mathrm{cbq}} + u_{\mathrm{cbd}} - u_{\mathrm{invbd}} \\ L\dfrac{di_{\mathrm{cbq}}}{dt} = -i_{\mathrm{cbq}}R - \omega L i_{\mathrm{cbd}} - u_{\mathrm{invbq}} \end{cases} \tag{22}$$

Where, u_{invad}, u_{invaq}, u_{invbd}, and u_{invbq} are the equivalent voltages of two inverters in the dq frame; i_{cad}, i_{caq}, i_{cbd}, and i_{cbq} are the equivalent currents of two traction arms in the dq frame. On the basis of (21) and (22), RPCs can be seen as two mutual coupled subsystems, each of them has two inputs and two outputs. Therefore, the linear quadratic state equation can be obtained, and there is

$$\begin{cases} \dot{\boldsymbol{x}} = \boldsymbol{A}\boldsymbol{x} + \boldsymbol{B}\boldsymbol{u} \\ \boldsymbol{y} = \boldsymbol{C}\boldsymbol{x} \end{cases} \tag{23}$$

In the equation above, there is

$$\boldsymbol{A} = \begin{bmatrix} -\frac{R}{L} & \omega & 0 & 0 \\ -\omega & -\frac{R}{L} & 0 & 0 \\ 0 & 0 & -\frac{R}{L} & \omega \\ 0 & 0 & -\omega & -\frac{R}{L} \end{bmatrix}, \boldsymbol{B} = \frac{1}{L}\begin{bmatrix} 1 & 0 & 0 & 0 \\ 0 & 1 & 0 & 0 \\ 0 & 0 & 1 & 0 \\ 0 & 0 & 0 & 1 \end{bmatrix}, \boldsymbol{C} = \boldsymbol{I}$$

$$\begin{aligned} \boldsymbol{u} &= \left[u_{\mathrm{cad}} - u_{\mathrm{invad}}, -u_{\mathrm{invaq}}, u_{\mathrm{cbd}} - u_{\mathrm{invbd}}, -u_{\mathrm{invbq}} \right]^{\mathrm{T}} \\ \boldsymbol{x} &= \left[i_{\mathrm{cad}}, i_{\mathrm{caq}}, i_{\mathrm{cbd}}, i_{\mathrm{cbq}} \right]^{\mathrm{T}} \end{aligned} \tag{24}$$

To achieve the dynamic active and reactive compensation, the optimal controller can be designed and the objective function can be described as

$$J' = \frac{1}{2}\int_0^{\infty} \left[\boldsymbol{e}^{\mathrm{T}}(t)\boldsymbol{Q}\boldsymbol{e}(t) + \boldsymbol{u}^{\mathrm{T}}(t)\boldsymbol{R}\boldsymbol{u}(t) \right] dt \tag{25}$$

Where, $\boldsymbol{e}(t)$ is the output error, $\boldsymbol{e}(t)=\boldsymbol{y}_d(t)-\boldsymbol{y}(t)$ and $\boldsymbol{y}_d(t)$ is the reference value of $\boldsymbol{y}(t)$. On the basis of the optimal control theory, the system must be observable. It can be judged by Rank Criteria, and there is

$$\operatorname{rank}\begin{bmatrix} \boldsymbol{C} \\ \boldsymbol{C}\boldsymbol{A} \\ \vdots \\ \boldsymbol{C}\boldsymbol{A}^{n-1} \end{bmatrix} = n \tag{26}$$

Hamilton function can be obtained

$$\begin{aligned} \boldsymbol{H}[\boldsymbol{x}, \boldsymbol{u}, \boldsymbol{\lambda}, t] = &\frac{1}{2}\left[(\boldsymbol{y}_d(t) - \boldsymbol{C}\boldsymbol{x} \right]^{\mathrm{T}} \boldsymbol{Q} \left[\boldsymbol{y}_d(t) - \boldsymbol{C}\boldsymbol{x} \right] \\ &+ \frac{1}{2}\boldsymbol{u}^{\mathrm{T}}\boldsymbol{R}\boldsymbol{u} + \boldsymbol{\lambda}^{\mathrm{T}}\left[\boldsymbol{A}\boldsymbol{x} + \boldsymbol{B}\boldsymbol{u} \right] \end{aligned} \tag{27}$$

Based on linear quadratic optimal control conditions, the equation (28) can be obtained, and there is

$$\begin{cases} \dfrac{\partial \boldsymbol{H}[\boldsymbol{x}, \boldsymbol{u}, \boldsymbol{\lambda}, t]}{\partial \boldsymbol{u}} = \boldsymbol{R}\boldsymbol{u} + \boldsymbol{B}^{\mathrm{T}}\boldsymbol{\lambda} = 0 \\ \dot{\boldsymbol{\lambda}} = -\dfrac{\partial \boldsymbol{H}(\boldsymbol{x}, \boldsymbol{u}, \boldsymbol{\lambda}, t)}{\partial \boldsymbol{x}} = -\boldsymbol{C}^{\mathrm{T}}\boldsymbol{Q}\boldsymbol{C}x + \boldsymbol{C}^{\mathrm{T}}\boldsymbol{Q}\boldsymbol{y}_d(t) - \boldsymbol{A}^{\mathrm{T}}\boldsymbol{\lambda} \\ \boldsymbol{u} = -\boldsymbol{R}^{-1}\boldsymbol{B}^{\mathrm{T}}\boldsymbol{\lambda} \end{cases} \tag{28}$$

By (28), the linear control law can be deduced, and there is

$$\begin{cases} \boldsymbol{K} = \boldsymbol{R}^{-1}\boldsymbol{B}^{\mathrm{T}}\boldsymbol{P} \\ \boldsymbol{u} = -\boldsymbol{K}\boldsymbol{x} + \boldsymbol{R}^{-1}\boldsymbol{B}^{\mathrm{T}}\boldsymbol{g} \\ \dot{\boldsymbol{x}} = \left[\boldsymbol{A} - \boldsymbol{B}\boldsymbol{K} \right]\boldsymbol{x} + \boldsymbol{B}\boldsymbol{R}^{-1}\boldsymbol{B}^{\mathrm{T}}\boldsymbol{g} \end{cases} \tag{29}$$

Where, $\boldsymbol{P}$ can be solved as Ricatti equation, and there is

$$\boldsymbol{P}\boldsymbol{A} + \boldsymbol{A}^{\mathrm{T}}\boldsymbol{P} - \boldsymbol{P}\boldsymbol{B}\boldsymbol{R}^{-1}\boldsymbol{B}^{\mathrm{T}}\boldsymbol{P} + \boldsymbol{C}^{\mathrm{T}}\boldsymbol{Q}\boldsymbol{C} = \boldsymbol{0} \tag{30}$$

The constant adjoint matrix $\boldsymbol{g}$ can be calculated as follows:

$$\boldsymbol{g} = (\boldsymbol{P}\boldsymbol{B}\boldsymbol{R}^{-1}\boldsymbol{B}^{\mathrm{T}} - \boldsymbol{A}^{\mathrm{T}})^{-1}\boldsymbol{C}^{\mathrm{T}}\boldsymbol{Q}\boldsymbol{y}_d \tag{31}$$

After defender 1's discrete defense ($S^*_{\mathrm{TSC}}, S^*_{\mathrm{TSR}}$) for the purpose of the cost function J_1 and defender 2's continuous defense ($I^*_{\mathrm{RPCp}}, I^*_{\mathrm{RPCqa}}, I^*_{\mathrm{RPCqb}}$) for the purpose of the cost function J_2, the sub-game perfect Nash equilibrium points ($S^*_{\mathrm{TSC}}, S^*_{\mathrm{TSR}}$ $I^*_{\mathrm{RPCp}}, I^*_{\mathrm{RPCqa}}, I^*_{\mathrm{RPCqb}}$) can be obtained, and the discrete and continuous elements can be executed by finite logic and optimal control, respectively. Nash equilibrium points can be described as follows:

$$\begin{cases} J_1(S^*_{\mathrm{TSC}}, S^*_{\mathrm{TSR}}, I^*_{\mathrm{RPCp}}, I^*_{\mathrm{RPCqa}}, I^*_{\mathrm{RPCqb}}) \le J_1(S_{\mathrm{TSC}}, S_{\mathrm{TSR}}, I^*_{\mathrm{RPCp}}, I^*_{\mathrm{RPCqa}}, I^*_{\mathrm{RPCqb}}) \\ J_2(S^*_{\mathrm{TSC}}, S^*_{\mathrm{TSR}}, I^*_{\mathrm{RPCp}}, I^*_{\mathrm{RPCqa}}, I^*_{\mathrm{RPCqb}}) \le J_2(S^*_{\mathrm{TSC}}, S^*_{\mathrm{TSR}}, I_{\mathrm{RPCp}}, I_{\mathrm{RPCqa}}, I_{\mathrm{RPCqb}}) \end{cases} \tag{32}$$

For one's own benefits, none has a deign to change one's strategy lonely. On the contrary, they would rather keep themselves in Nash equilibrium points where it is in an optimal compensation mode for all compensation elements, including active or passive elements, continuous elements or discrete elements, such as RPCs, TSCs or TSRs. To this end, the dynamic hybrid compensator can be cooperatively controlled to maintain the three-phase current balanced for any unfriendly attacks. The dynamic hybrid control diagram shown in Fig. 9.

In a word, the traction power system can be seen as a dynamic game between two classes of players: one class is the attackers, who firstly break the current balance through the loads stochastic jumps; then, the other is the dynamic hybrid compensator, including defender 1 (TSCs and TSRs) and defender 2 (RPCs), based on the shared information, can be cooperatively controlled to maintain the three-phase balanced for any unfriendly attacks by the criteria of "Nash equilibrium".

V. Simulation and Experiment Verification

To verify the structure and control method in the paper, simulations and experiments have been carried out. The simulation for the high-speed electrified traction system is given by PSIM 9.0 (time step is 1E-005) and the schematic diagram is shown in Fig.4, where three-phase voltage of the system is 220kV and the frequency is 50Hz. The ratio of step-down transformer is 27.5kV to 2.82kV. There are 10 sets of RPC module, and the capacity of each RPC module is 1.92MVA.

Considering the power system as shown in Table V, the matrix $\boldsymbol{Q}$ and $\boldsymbol{R}$ can be given as follows:

$$\boldsymbol{Q} = \begin{bmatrix} 1 & 0.5 & 0 & 0 \\ 0.5 & 1 & 0 & 0 \\ 0 & 0 & 1 & 0.5 \\ 0 & 0 & 0.5 & 1 \end{bmatrix}, \boldsymbol{R} = \begin{bmatrix} 1 & 0 & 0 & 0 \\ 0 & 1 & 0 & 0 \\ 0 & 0 & 1 & 0 \\ 0 & 0 & 0 & 1 \end{bmatrix} \tag{33}$$

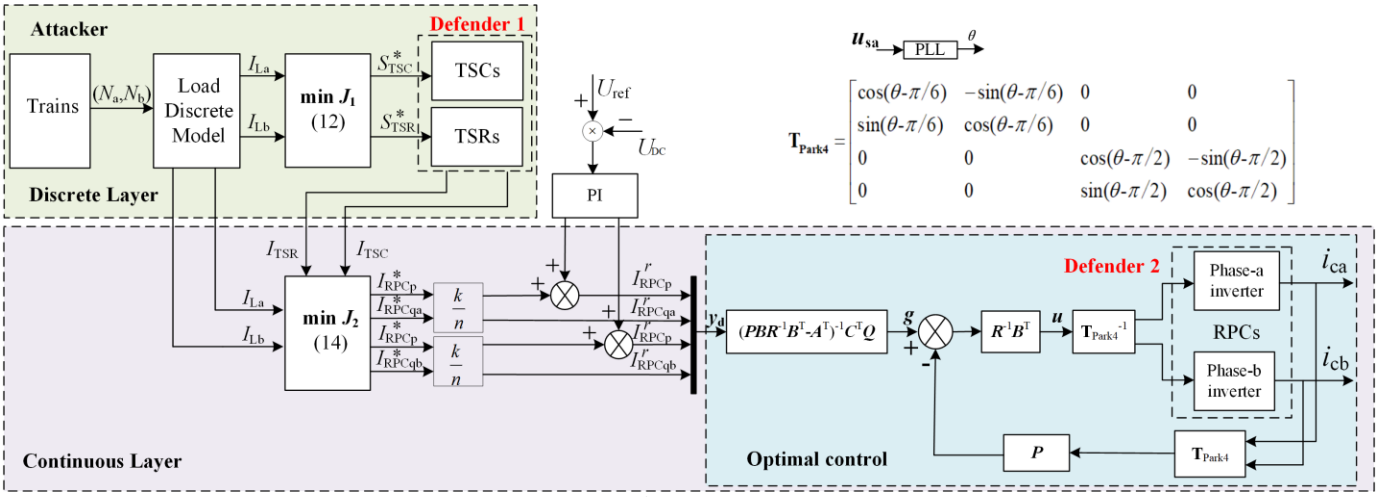

Fig. 9. The control diagram of the two-level optimized hybrid control.

Based on (30), $\boldsymbol{P}$ can be solved

$$\boldsymbol{P}=\begin{bmatrix}\boldsymbol{P}_1 & \boldsymbol{0}\\ \boldsymbol{0} & \boldsymbol{P}_1\end{bmatrix}=\begin{bmatrix}0.0022 & 0.0004 & 0 & 0\\ 0.0004 & 0.0026 & 0 & 0\\ 0 & 0 & 0.0022 & 0.0004\\ 0 & 0 & 0.0004 & 0.0026\end{bmatrix}. \quad (34)$$

By (29), the control law of RPCs can be obtained. As the characteristic roots of system are -498.75+295.55i, -498.75-295.55i and the real components of characteristic roots are negative, so the control system of RPCs is effective and stable. Similarly, the setting process of experimental parameters for RPCs is designed as the same, and the specific control parameters are shown in Table V.

Table V
System Parameters

COMPONENTS	PARAMETERS	SIMULATION	EXPERIMENT
Trains	S	9.6 MVA	10KVA
TSRs	$L1$	0.869 H	53.395 mH
	$L2$	0.869 H	53.395 mH
	$L3$	0.4345 H	26.697 mH
	$L4$	0.2172 H	13.348 mH
TSCs	$C1$	11.669uF	0.19 mF
	$C2$	11.669uF	0.19 mF
	$C3$	23.338uF	0.38 mF
	$C4$	46.676uF	0.76 mF
RPCs	SUB-MODULE	10	5
	C	80mF	10 mF
	L	1mH	1.5mH
	U_{DC}	5.0KV	400 V
	f_c	1KHz	4KHz
	$\boldsymbol{P}_1$	$\begin{bmatrix}0.0022 & 0.0004\\ 0.0004 & 0.0026\end{bmatrix}$	$\begin{bmatrix}0.0025 & 0.0003\\ 0.0003 & 0.0015\end{bmatrix}$

A. Simulation Analysis

As the trains go through the railway system randomly, TSRs, TSCs and RPCs should accomplish the dynamic compensation appropriately for all probable train loads. To verify the dynamic performance of the hybrid compensator, the train load jumps on two traction arms are dynamically simulated.

Firstly, a train enters into phase-a traction power arm and the currents of the train loads are shown in Fig. 10(a). If no defender takes an action, the three-phase grid currents will be unbalanced. Based on attacker's attack and the two-level optimized control method, TSCs and TSRs (defender 1) can take an action for minimizing the cost function J_1, shown in Fig. 10(b), where TSC1 and TSR1 have been switched on. Then, RPCs (defender 2), based on the train load jump and defender 1's action, are optimally controlled to minimize the cost function J_2, shown in Fig. 10(c). As a result, the current waveforms of three-phase grid are basically balanced, shown in Fig. 10 (d). So, after the dynamic game, defender 1 and defender 2 have quickly reached to "Nash equilibrium" points to achieve the optimal compensation. In addition, the capacitor voltage of each RPC can be kept at 5.0 kV, shown in Fig. 10(e).

Then, at 0.4s, another train enters into phase-b traction power arm. The original defense that TSC1 and TSR1 switched on is no longer suitable for defending the load jump. Furthermore, defender 1 take an action that TSC3 and TSR3 have switched on and defender 2 is not required in this period, more detailed information shows in Fig. 10. More train jumps of the attacker have been simulated at 0.8s, 1.2s and 1.6s. Regardless the train load jumps, TSRs, TSCs can be wisely auto-switched, and RPCs can be cooperatively controlled to minimize the unbalanced level. So, it can be proved that the two-level optimized hybrid controller can keep the compensation system working in an optimal mode for any train-load jump attack.

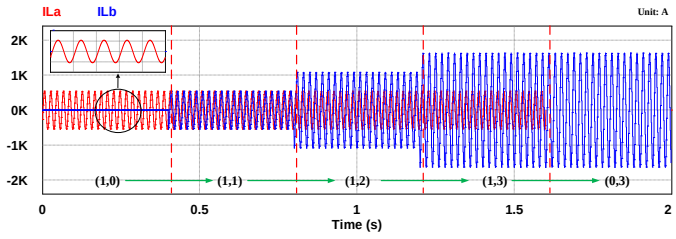

(a)

This article has been accepted for publication in a future issue of this journal, but has not been fully edited. Content may change prior to final publication. Citation information: DOI 10.1109/TPEL.2018.2887226, IEEE Transactions on Power Electronics

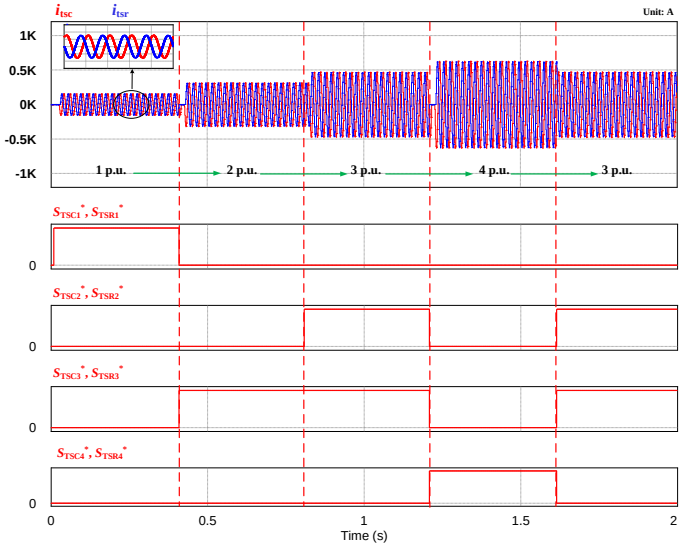

(b)

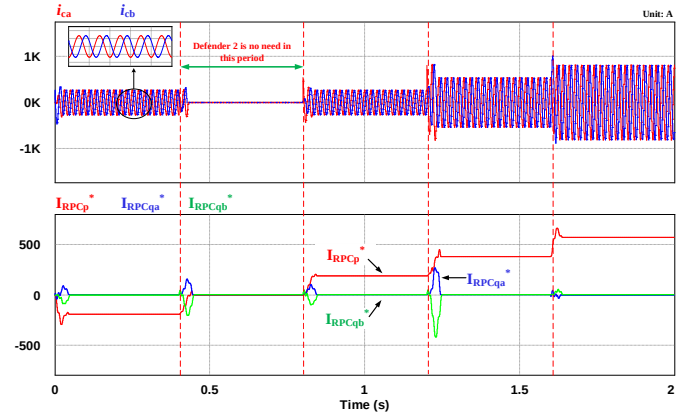

(c)

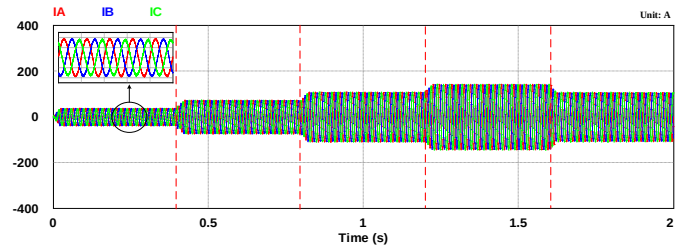

(d)

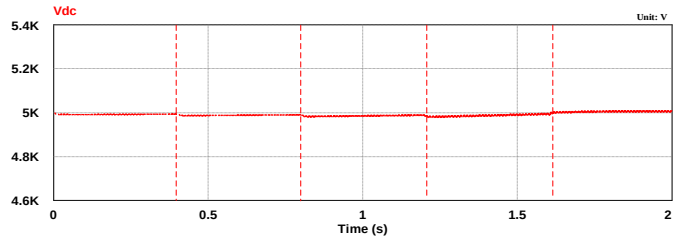

(e)

Fig. 10. Current waveforms with train load stochastic jump. (a) The currents of the train loads. (b) The currents of TSCs and TSRs. (c) The output currents of RPCs. (d) The currents of the three-phase grid. (e) The capacitor voltage of RPC.

Due to a probable fault of RPCs, the optimal compensation in bad conditions is simulated. At first, there are 4 trains are in phase-a traction arm and no train is in phase-b traction arm, shown in Fig. 11(a). The hybrid compensator is good (ς =100%) and the three-phase grid currents are fully balanced, shown in Fig. 11(b). While at 0.2s, one set of RPCs falls toward a fault (ς =90%) and the hybrid system can only optimally compensate by the two-level optimized hybrid controller. At this moment, defender 1(TSCs, TSRs) is no change and defender 2 (RPCs) can optimally compensate by (19) in spite of the fault, the currents of which can be shown in Fig. 11(c), (d). As a result, the three-phase grid currents are mostly balanced and the capacitor voltage of RPCs is kept at 5kV as well, shown in Fig. 11(b), (e). Meanwhile, at 0.3s, 3 sets of RPCs fall toward a fault (ς =70%). According to (16)-(19), the unbalanced three-phase currents are unavoidable and the hybrid compensator can do a maximum struggle to optimally compensate, shown in Fig. 11(b), (c), (d). So, it can be found that the hybrid controller can optimally compensate in bad conditions.

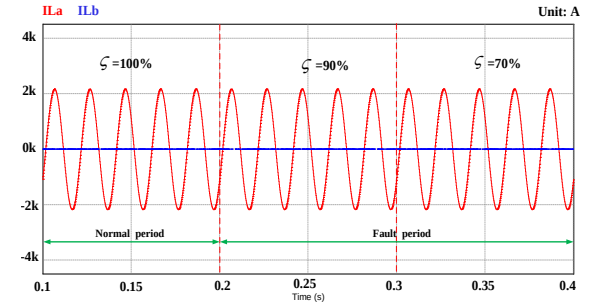

(a)

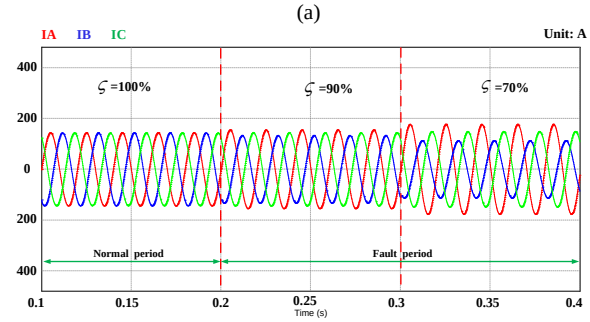

(b)

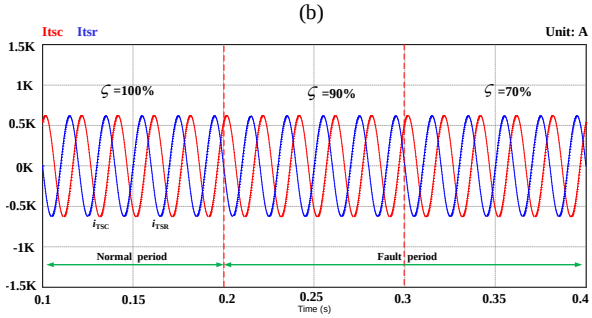

(c)

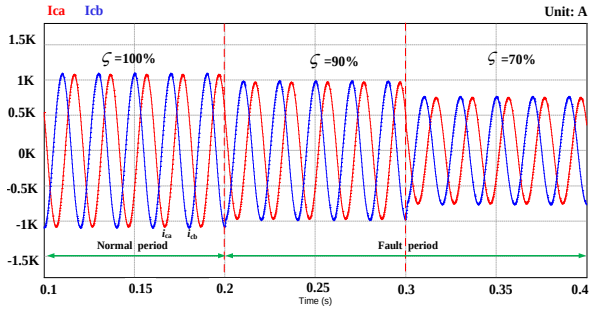

(d)

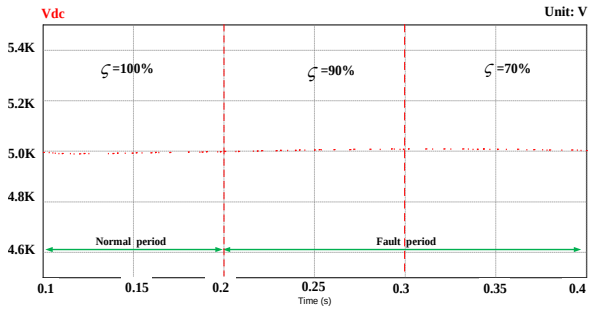

(e)

Fig. 11. Waveforms towards a fault of RPCs in the extreme case (4,0). (a) The currents of the train loads. (b)The currents of the three-phase grid. (c) The currents of TSCs and TSRs. (d) The currents of RPCs. (e) The capacitor voltage of RPC.

B. Experiments

The experimental prototype has been built in Lab and the prototype diagram is illustrated in Fig 12. It mainly includes several elements: the traction transformer, RPCs, TSCs, TSRs, linear load. The digital control system can be realized by DSP and FPGA. The pictures of the prototype system are shown as Fig.13. Fig.13 (a) shows V/v traction power system and Fig.13 (b) shows simulated load array and TSCs, TSRs' trigger board. In addition, Fig.13 (c) is the prototype of RPC and Fig.13 (d) is DSP control board and Power Module. The prototype parameters of hybrid compensator are listed in Table V.

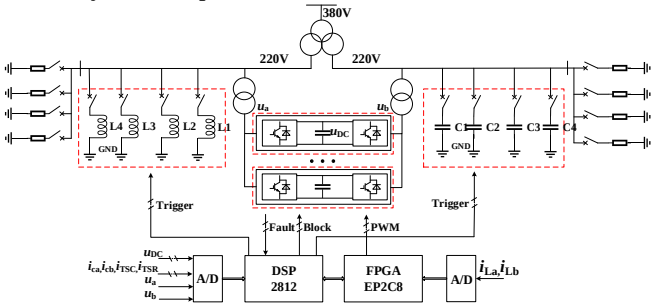

Fig. 12. The implementation diagram of the device.

Fig. 13. The picture of the prototype system. (a) V/V traction power system. (b) The simulated train load jump array and TSCs, TSRs trigger boards. (c) RPC's prototype. (d) DSP control board and Power module.

To prove the compensation capacities and the control performance of the hybrid compensator, a dynamic operation of the locomotive loads is simulated from (4,1) to (4,0). At first, four trains in phase-a traction arm and one train in phase-b traction arm (attackers' action), the currents of the train loads are shown in Fig. 14(a). TSC1, 4 and TSR1, 4 of defender 1 are switched on simultaneously, shown in Fig. 14(c), (d). Based on (17)-(19), RPCs of defender 2 are controlled to output and reach the expecting currents. Here, the currents of a submodule and the other modules of RPCs are displayed in Fig. 14(e). And the dc-link voltage of dc-link is kept stable at 400V, shown in Fig. 14(f). Finally, by the hybrid compensator, three-phase grid currents are kept in balance, shown in Fig. 14(b).

At 60ms, one submodule of RPCs falls toward a fault and its current is suddenly reduced to zero, shown in Fig. 14(e). At this moment, the residual rate of RPCs' capacity ς is reduced to 80%. As TSCs and TSRs work as well, so the compensating stress of RPCs is alleviated and the three-phase grid currents could be still controlled in the balance in spite of a little fault of RPCs. At 140ms, one train leaves from phase-b traction arm. The power demands are the largest and the system can't be fully compensated any longer. By the two-level hybrid controller, TSC1, TSR1 are auto-switched off and TSC4, TSR4 are still on. According to (16)-(19), RPCs can only optimal compensate by the K-T points ($I^*_{\mathrm{RPCp}}, I^*_{\mathrm{RPCqa}}, I^*_{\mathrm{RPCqb}}$). To this end, the three-phase grid currents are controlled in the minimal imbalance, shown in Fig. 14(b). The current outputs of RPCs, TSCs and TSRs are always keeping in the optimal compensation state and they are cooperatively controlled by "Nash equilibrium" points.

So, the hybrid system composed of TSCs, TSRs, and RPCs is an effective method to enhance the dynamic compensation capacities and the hybrid system can be cooperatively controlled to minimize the unbalanced level of three-phase grid currents by the two-level optimized hybrid controller.

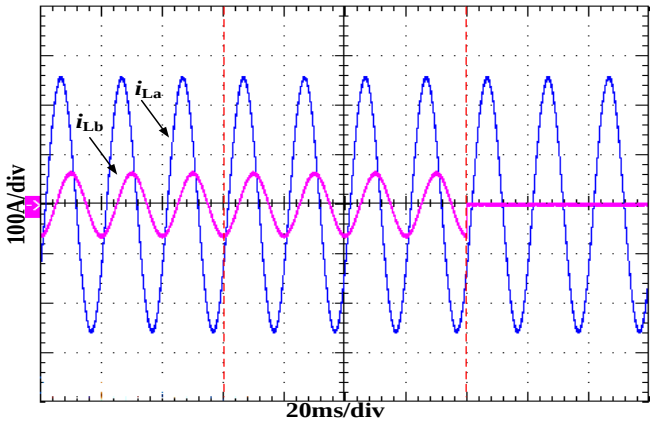

(a)

This article has been accepted for publication in a future issue of this journal, but has not been fully edited. Content may change prior to final publication. Citation information: DOI 10.1109/TPEL.2018.2887226, IEEE Transactions on Power Electronics

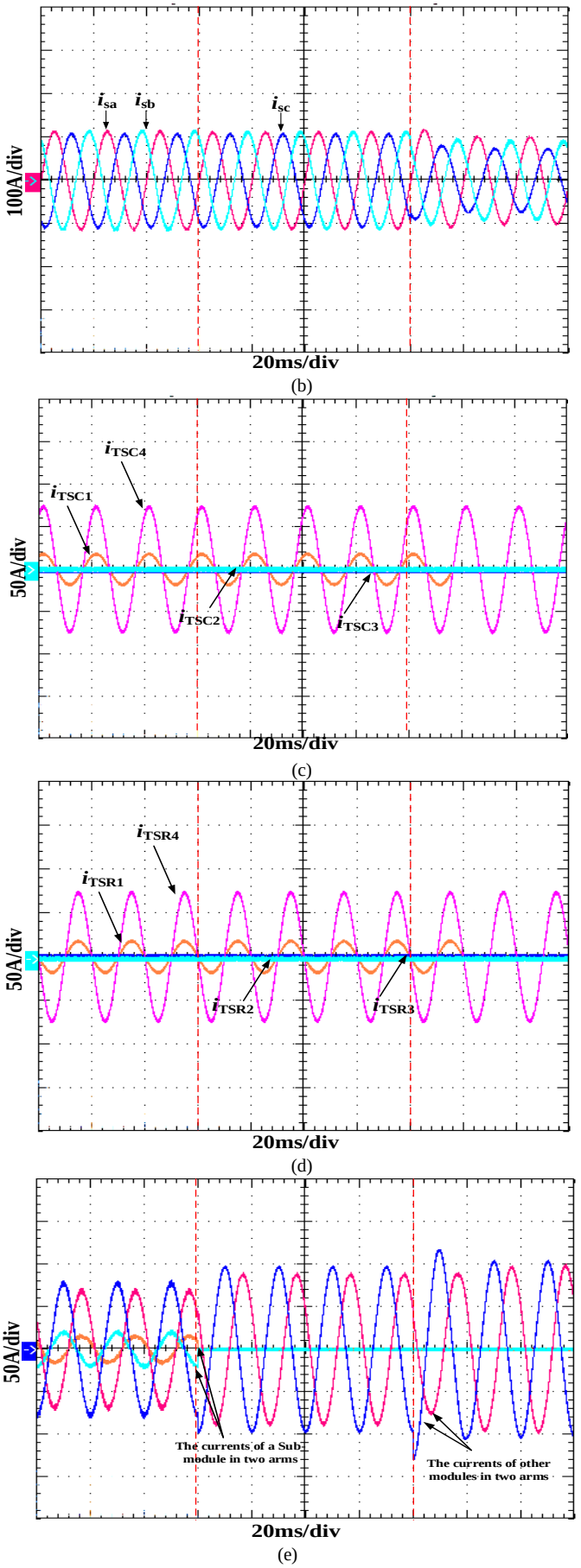

Fig. 14. Experimental waveforms of the hybrid compensation system. (a) The currents of the train loads. (b)The currents of the three-phase grid. (c) The currents of TSCs. (d) The currents of TSRs. (e) The currents of RPCs. (f) The capacitor voltage of RPCs.

VI. Conclusions

In this paper, firstly the stochastic train loads and the power compensation demands for China V/v high-speed railway system are listed and analyzed. Secondly, to enhance the dynamic compensation capacities, a hybrid scheme composed of RPCs, TSCs and TSRs is studied. Then, based on the game theory, a two-level coordinated hybrid controller for the dynamic compensator is proposed and implemented. What's more, if a part of RPCs falls toward a fault, the hybrid controller can compensate optimally. Finally, simulations and experiments are implemented to prove the capacities of the hybrid system and the dynamic performance of the hybrid controller.

References

[1] Shu, Zeliang, S. Xie, and Q. Li. "Single-Phase Back-To-Back Converter for Active Power Balancing, Reactive Power Compensation, and Harmonic Filtering in Traction Power System." *IEEE Transactions on Power Electronics.*, vol. 26, no. 2, pp. 334-343,2011.

[2] Wang, Jinhao, et al. "Analysis of power quality issues of electrified railway." *International Conference on Mechanical and Intelligent Manufacturing Technologies* IEEE, 179-182. 2017.

[3] Oettmeier, Martin, Volker Staudt., et al. "Dead-Beat Control Algorithm for Single-Phase 50-kW AC Railway Grid Representation." *IEEE Transactions on Power Electronics* 25.5(2010):1184-1192.

[4] S. M. M. Gazafrudi, A. Tabakhpour Langerudy, E. F. Fuchs, and K. Al-Haddad, "Power quality issues in railway electrification: A comprehensive perspective," *IEEE Trans. Ind. Electron.*, vol. 62, no. 5, pp. 3081–3090, May 2015.

[5] D. Zhang, Z. Zhang, W. Wang, and Y. Yang, "Negative sequence current optimizing control based on railway static power conditioner in V/v traction power supply system," *IEEE Trans. Power Electron.*, vol. 31, no. 1, pp. 200–212, Jan. 2016.

[6] Hu, Haitao, et al. "Harmonic Resonance Evaluation for Hub Traction Substation Consisting of Multiple High-speed Railways." *IEEE Transactions on Power Delivery* PP.99(2017):1-1.

[7] Ronanki, Deepak, and S. S. Williamson. "Evolution of Power Converter Topologies and Technical Considerations of Power Electronic Transformer based Rolling Stock Architectures." *IEEE Transactions on Transportation Electrification* PP.99:1-1. 2018.

[8] Lao, Keng Weng, et al. "Analysis of the Effects of Operation Voltage Range in Flexible DC Control on Railway HPQC Compensation Capability in High-Speed Co-phase Railway Power." *IEEE Transactions on Power Electronics* 33.2:1760-1774. 2018.

[9] Steimel A. "Power-electronic grid supply of AC railway systems." *International Conference on Optimization of Electrical & Electronic Equipment IEEE*, 2012.

[10] Krah, J. O, and J. Holtz. "Total compensation of line-side switching harmonics in converter-fed AC locomotives." *IEEE Transactions on Industry Applications*, 31.6:1264-1273. 1995.

[11] Zhao, C., Dujic, D., Mester, A., Steinke, J. K., Weiss, M., & Lewdeni-Schmid, S., et al. "Power electronic traction transformer—medium voltage prototype." *IEEE Transactions on Industrial Electronics*, 61(7), 3257-3268. 2014.

[12] Drazen Dujic, Chuanhong Zhao, Akos Mester, et al. "Power Electronic Traction Transformer-Low Voltage Prototype." *IEEE Transactions on Power Electronics*,26.12: 5522-5534. 2014.

[13] Aceiton, Roberto, J. Weber, and S. Bernet. "Input Filter for a Power Electronics Transformer in a Railway Traction Application." *IEEE Transactions on Industrial Electronics* PP.99(2018):1-1.

[14] Feng, Jianghua, et al. "Power Electronic Transformer-Based Railway Traction Systems: Challenges and Opportunities." *IEEE Journal of Emerging & Selected Topics in Power Electronics* 5.3(2017):1237-1253.

[15] H. Hu, Z. He, and S. Gao, "Passive filter design for china high-speed railway with considering harmonic resonance and characteristic harmonics," *IEEE Trans. Power Del.*, vol. 30, no. 1, pp. 505–514, Feb. 2015.

[16] G. Celli, F. Pilo, and S. B. Tennakoon, "Voltage regulation on 25 kV AC railway systems by using thyristor switched capacitor," in *Proc. 9th Int. Conf. Harmonics Qual. Power*, vol. 2, pp. 633–638, 2000.

[17] R Grunbaum, J. -Ph. Hasler, T. Larsson, and M. Meslay, "STATCOM to enhance power quality and security of rail traction supply," in *Proc. 8th Int. Symp. Adv. ElectroMech. Motion Syst. Elect. Drives*, pp. 1–6, 2009.

[18] T. Pee-Chin, L. P. Chiang, and D. G. Holmes, "A robust multilevel hybrid compensation system for 25-kV electrified railway applications," *IEEE Trans. Power Electron.*, vol. 19, no. 4, pp. 1043–1052, Jul. 2004.

[19] Bahrani, Behrooz, and A. Rufer. "Optimized -Based Voltage Support in Traction Networks Using Active Line-Side Converters." *IEEE Transactions on Power Electronics* 28.2(2013):673-685.

[20] Y. Mochinaga, Y. Hisamizu, M. Takeda, T. Miyashita and K. Hasuike, "Static power conditioner using GTO converters for AC electric railway," *Conference Record of the Power Conversion Conference* - Yokohama 1993, Yokohama, Japan, 1993, pp. 641-646.

[21] Z. Sun, X. Jiang, D. Zhu, and G. Zhang, "A novel active power quality compensator topology for electrified railway," *IEEE Trans. Power Electron.*, vol. 19, no. 4, pp. 1036–1042, Jul. 2004.

[22] Y. Horita, N. Morishima, M. Kai, M. Onishi, T. Masui, and M. Noguchi, "Single-phase STATCOM for feeding system of Tokaido Shinkansen," in *Proc. Int. Power Electron. Conf. (IPEC)*, 2010, pp. 2165–2170.

[23] T. S. Win, B. Yusuke, E. Hiraki, T. Tanaka, and M. Okamoto, "A half-bridge inverter based active power quality compensator using a constant dc capacitor voltage control for electrified railways," in *Proc. 7th Int. Power Electron. Motion Control Conf. (IPEMC)*, 2012, vol. 1, pp. 314–320.

[24] Q. Wu, Q. Jiang, and Y. Wei, "Study on railway unified power quality controller based on STATCOM technology," in *Proc. 5th Int. Power Eng. Optim. Conf. (PEOCO)*, 2011, pp. 297–300.

[25] F. Ma *et al.*, "A railway traction power conditioner using modular multilevel converter and its control strategy for high-speed railway system," *IEEE Trans. Transp. Electrification*, vol. 2, no. 1, pp. 96–109, Mar. 2016.

[26] Song P, Lin J, Li Y, et al, "PIR Control Strategy on Compensation of Negative Sequence and Harmonic for Railway Power Supply System Using MMC-RPC," *Transactions of China Electrotechnical Society*, 2017.

[27] Zhao Y, Dai N Y, BaoAn, "Application of three-phase modular multilevel converter (MMC) in co-phase traction power supply system," *Transportation Electrification Asia-Pacific. IEEE*, 2014, pp:1-6.

[28] Hu, Sijia, et al. "A Comprehensive Study for The Power Flow Controller Used in Railway Power Systems." *IEEE Transactions on Industrial Electronics.* vol. 65, no. 8, pp. 6032-6043, Aug. 2018.

[29] Roudsari, Hossein Mahdinia, A. Jalilian, and S. Jamali. "Flexible Fractional Compensating Mode for Railway Static Power Conditioner in V/v Traction Power Supply System." *IEEE Transactions on Industrial Electronics* PP.99(2018):1-1.

[30] B. C. Chen, C. M. Zhang, W. J. Zeng, C. H. Tian, and J. X. Yuan, "An electrical-magnetic hybrid power quality compensation strategy for V/V traction power supply system," *Proc. IEEE Energy Convers. Congr. Expo.*,2014, pp. 3774–3779.

[31] A. Luo, C. Wu, J. Shen, Z. Shuai, and F. Ma, "Railway static power conditioners for high-speed train traction power supply systems using three-phase V/V transformers," *IEEE Trans. Power Electron.*, vol. 26, no. 10, pp. 2844–2856, Oct. 2011.

[32] S. Hu *et al.*, "A new railway power flow control system coupled withasymmetric double LC branches," *IEEE Trans. Power Electron.*, vol. 30, no. 10, pp. 5484–5498, Oct. 2015.

[33] B. Chen, C. Zhang, C. Tian, J. Wang, and J. Yuan, "Negative sequence current optimizing control based on railway static power conditioner in V/v traction power supply system," *IEEE Trans. Power Electron.*, vol. 31, no. 6, pp. 2079–2091, Jun. 2016.

[34] K. Lao, M. Wong, N. Dai, C. Wong, and C. Lam, "A systematic approach to hybrid railway power conditioner design with harmonic compensation." *IEEE Trans. Ind. Electron.*, vol. 62, no. 2, pp. 1831–1839, Feb. 2015.

[35] Bonan An, Yong Li, Fang Liu, Bin Xie, Sijia Hu, et al., "An Asymmetrical Connection Balance Transformer-Based Hybrid Railway Power Conditioning System With Cost-Function Optimized." *IEEE Trans. Power Electron.* vol. 4, no. 2, pp. 577-599, Jun. 2018.

[36] Xie, Bin, et al., "A Compensation System for Co-Phase High-Speed Electric Railways by Reactive Power Generation of SHC&SAC." *IEEE Transactions on Industrial Electronics* PP.99(2018):1-1.

[37] M Arabahmadi, M Banejad, A li Dastfan, "Hybrid Traction Power Quality Compensation System in Electrified Railway for Nominal Rating Reduction of Three-Phase Converter Power Switches." *8th Power Electronics, Drive System & Tchnologied Conference*(PEDSTC). 2017, pp. 478-483.

[38] L Luo, Y Chang, Y Li, "A Hybrid Power Conditioner for Co-Phase Power Supply System and Its Capacity Analysis," IEEE. 2017, pp. 510-515.

[39] Rahmani, Salem, et al. A Combination of Shunt Hybrid Power Filter and Thyristor-Controlled Reactor for Power Quality." *IEEE Transactions on Industrial Electronics* 61.5:2152-2164. 2014.

[40] BERGSTRA. JA, MIDDELBURG. CA, "Continuity controlled hybrid automata." *Journalof Logic and Algebriac Programming*, 2006, (68): 1-2,5-53.

[41] BELKACEM SAIT, HASSANE ALLA, "Modelling by Hybrid Petri nets in dynamic electrical systems." *WSEAS Transactions on Systems*, 2006, 5(11):2606-2611.

[42] Michael S. Branicky, Vivek S. Borkar, and Sanjoy K. Mitter, "A unified framework for hybrid control: Model and optimal control theory", *IEEE Transactions on Automatic Control*, vol. 43, no. 1, pp. 31–45, 1998.

[43] A. Nerode and W. Kohn, "Multiple agent hybrid control architecture", in Hybrid Systems, Robert L.Grossman, Anil Nerode, Anders P. Ravn, and Hans Rischel, Eds., pp. 297–316. Springer Verlag, New York, 1993.

[44] P.E. Caines and Y.J. Wei, "Hierarchical hybrid control systems: A lattice theoretic formulation", *IEEE Transactions on Automatic Control*, vol. 43, no. 4, pp. 501–508, April 1998.

[45] R. Deng, Z. Yang, M.-Y. Chow, and J. Chen, "A survey on demand response in smart grids: Mathematical models and approaches," *IEEE Trans. Ind. Informat.*, vol. 11, no. 3, pp. 570–582, Jun. 2015.

[46] Mei, Shengwei, W. Wei, and F. Liu. "On engineering game theory with its application in power systems." *Control Theory & Technology*.15.11-12, 2017.

[47] Abobakr, Saad A., W. H. Sadid, and G. Zhu. "Game-Theoretic Decentralized Model Predictive Control of Thermal Appliances in Discrete-Event Systems Framework." *IEEE Transactions on Industrial Electronics*.pp.99:1-1, 2018.

[48] Z. Zhu, S. Lambotharan, W. H. Chin, and Z. Fan, "A game theoretic optimized framework for home demand management incorporating local energy resources," *IEEE Trans. Ind. Informat.*, vol. 11, no. 2, pp. 353–362, Apr. 2015.

[49] E. R. Stephens, D. B. Smith, and A. Mahanti, "Game theoretic model predictive control for distributed energy demand-side management," *IEEE Trans. Smart Grid*, vol. 6, no. 3, pp. 1394–1402, May 2015.

[50] An Luo, Fujun Ma, Chuanping Wu, Shi Qi Ding, Q. -C. Zhong, Zhi Kang Shuai, "A Dual-Loop Control Strategy of Railway Static Power Regulator Under V/V Electric Traction System," *IEEE Trans. Power Electronics*, Vol.26, no.7, pp.2079 – 2091, 2011.

Zhen Zhu was born in Hunan, China, 1988. He received the B.S. degree and the M.S. degree in Automation from College of Geophysics and Information Engineering, China University of Petroleum, Beijing, China, in 2013 and 2017, respectively. He has been working toward the Ph.D. degree in Electrical Engineering in the College of Electrical and Information Engineering, Hunan University, Changsha since 2017. His research interests include hybrid compensation of traction system and energy management of energy router.

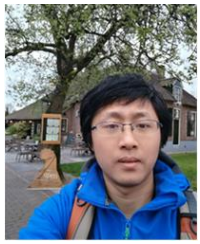

Fujun Ma (M'15) was born in Hunan, China, 1985. He received the B.S. degree in Automation and Ph.D. degree in Electrical Engineering from Hunan University, Changsha, in 2008 and 2015, respectively.

Since 2016, he has been an Associate Professor with the College of Electrical and Information Engineering, Hunan University. His research interests include power quality managing technique of electrified railway, electric power saving, reactive power compensation, and active power filters.

Xin Wang was born in Anhui, China, 1995. He received the B.S degree from China University of Mining and Technology, Jiangsu, China, in 2017. He is currently working toward the M.S degree in the College of Electrical and Information Engineering, Hunan University, Changsha, China.

His research interests include analysis, model and optimization of dc converter.

Lingfeng Deng was born in Jiangxi, China, 1995. He received the B.S. degree from College of Electrical and Power Engineering, China University of Mining and Technology, Xuzhou, China, in 2018. He is currently working toward the M.S. degree in the College of Electrical and Information Engineering, Hunan University, Changsha, China.

His research interests include power quality management and modular multilevel converter.

Gaoxiang Li was born in Henan, China, 1990. He received the B.S. degree from the School of Electrical Engineering and Automation, Henan Polytechnic University, Jiaozuo, China, in 2014. He received the M.S. degree from the College of Information science and Engineering, Central South University, Changsha, China, in 2017. he is currently working toward the Ph.D. degree in the College of Electrical and Information Engineering, Hunan University. His research interests include power quality control, new energy generation, sub-synchronous oscillation suppression.

Xinwei Wei was born in Henan, China, 1990. He received the B.S. degree from the School of Electrical Engineering and Automation, Henan normal University, Xinxiang, China, in 2014. He received the M.S. degree from the College of Information science and Engineering, Changsha University of Science & Technology, Changsha, China, in 2017. he is currently working toward the Ph.D. degree in the College of Electrical and Information Engineering, Hunan University. His research interests include power amplifier and adaptive switching control for underwater electroacoustic transduction system.

Yuxuan Tang was born in Jiangsu, China, 1995. She received the B.S degree from Northwest Minzu University, Gansu, China, in 2018. She is currently working toward the M.S. degree in the College of Electrical and Information Engineering, Hunan University, Changsha, China.

Her research interests include power quality managing technique of electrified railway and modular multilevel converter

Siyi Liu was born in Hubei, China, 1997. She received the B.S. degree from College of Information and Control Engineering, China University of Petroleum, Huadong, China, in 2018. She is currently working toward the M.S. degree in the College of Electrical and Information Engineering, Hunan University, Changsha, China.

Her research interests include microgrid energy storage and instantaneous energy conversion power supply.